Lung Vessel Enhancement in Low-Dose CT Scans – The LANCELOT Method

Nico Merten[1,2], Kai Lawonn[3], Philipp Gensecke[4], Oliver Großer[4], Bernhard Preim[1,2]

[1]Research Campus STIMULATE
[2]Department of Simulation and Graphics, Otto-von-Guericke University
[3]Institute for Computational Visualistics, University of Koblenz-Landau
[4]Department of Radiology and Nuclear Medicine, University Hospital Magdeburg

Abstract

To reduce the patient's radiation exposure from computed tomography scans (CT), low-dose CT scans can be recorded. Several image processing methods exist to segment or enhance the lung blood vessels from contrast-enhanced or high resolution CT scans, but the reduced contrast in low-dose CT scans leads to over- or under-segmentation. Our *LANCELOT* method combines maximum response and stick filters to enhance lung blood vessels in native, low-dose CT scans. We compare our method with the vessel segmentation and enhancing methods from Frangi and Sato et al. Our method has two advantages that were confirmed in an evaluation with two clinical experts: First, our method enhances small vessels and vessel branches more clearly and second, it connects vessels anatomically correct, while the others create discontinuities.

1   Introduction

For a long time, the most important imaging methods for the detection of lung nodes were chest radiographs (CXRs). Compared to computed tomography scans (CTs), CXRs suffer from occlusion problems and are not able to reproduce as much contrast as CT scans are able to [National Lung Screening Trial Research Team, 2011]. On the other hand, the radiation exposure during CT examinations is significantly higher. One way of reducing the patient's exposure to radiation is to take low-dose CT scans instead of diagnostic CTs, which leads to lower image contrast. Another possibility is the administration of contrast agent to emphasize blood vessels.

Several image processing methods are available for segmentation or enhancement of blood vessels from CT angiography (CTAs) diagnostic CT scans. Sato and Frangi et al. combine an evaluation of the Hessian matrix eigenvalues and a priori knowledge about the vessel and background brightness to enhance vessel-like structures in angiography scans [Sato, Y and Nakajima, S and Atsumi, H et al., 1997, Frangi, A F and Niessen, W J and Vincken, K et al., 1998]. Alternatively, if high resolution CT scans are available, 3D region growing allows the extraction of blood vessels [Kuhnigk, J-M and Hahn, H and Hindennach, M et al., 2003]. We refer to the *VESSEL12 Study* by Rudyanto et al. [Rudyanto, R D and Kerkstra, S and Van Rikxoort, E M et al., 2014] for a detailed comparison of automated lung vessel segmentations in CT scans.

The aforementioned approaches produce convincing results for the image scans they were applied to, but we were not able to reproduce comparable results when applying them to low-dose CT scans. Using thresholding or region growing leads either to over- or under-segmentation and evaluating the Hessian Matrix is also not sufficient. While larger vessels are enhanced, many medium and small vessels are not. Furthermore, although visibly connected in the original scan, some vessels are separated since the contrast between them and parenchyma is too low in low-dose CT recordings. For that reason, we present our lung vessel enhancement method for low-dose CT scans, LANCELOT in short.

2   Materials and Methods

In the following we abbreviate image coordinates, e.g. $I(x, y, z)$, by $I(\mathbf{x})$. Sato and Frangi et al. use multi-scale line enhancement filters to segment blood vessels in contrast-enhanced and native CT scans [Sato, Y and Nakajima, S and Atsumi, H et al., 1997, Frangi, A F and Niessen, W J and Vincken, K et al., 1998]. First, a Gaussian convolution $G(\mathbf{x}; \sigma)$ is applied to reduce image noise. Then, the Hessian matrix $H(\mathbf{x})$ is set up for $I(\mathbf{x})$ and its eigenvalues λ_1, λ_2, and λ_3 are evaluated. This yields

$$H(\mathbf{x}; \sigma) = H(I(\mathbf{x}) * G(\mathbf{x}; \sigma)) \tag{1}$$

To find the brighter blood vessels in the dark parenchyma, the conditions

$$(\lambda_1 \approx 0) \wedge (\lambda_2 \approx \lambda_3 \ll 0) \tag{2}$$

1

must hold. To separate lines from sheet-like and blob-like shapes such as skin and noise components, respectively, a vesselness function evaluates how good these conditions are fulfilled. This function is called $\lambda_{123}(\mathbf{x}; \sigma)$.

These conditions are combined with 3D multi-scale filters. When multi-scale filters are applied, individual filter responses are first normalized and then the maximum response is added to $I(\mathbf{x})$. The result image $I'(\mathbf{x})$ is given by

$$I'(\mathbf{x}) = I(\mathbf{x}) + \max_{1 \leq i \leq n} (\sigma_i^2 \cdot \lambda_{123}(\mathbf{x}; \sigma_i)) \tag{3}$$

where n donates the number of multi-scale filters. For each multi-scale filter the vesselness measure is normalized with σ_i^2 from the Gaussian convolution.

We combine this maximum response approach with the *Stick* kernels from Czerwinski et al. [Czerwinski, R N and Jones, D L and O'brien, W D, 1998]. To create filter kernels of varying sizes, we use the Bresenham algorithm [Bresenham, J E, 1965]. This results in $filterRadius \times 4$ individual filter kernels. As presented in Figure 1, for $filterRadius = 2$ this results in 8 individual kernels. In the following we abbreviate $filterRadius \times 2 + 1 = m$. For every image pixel $I(\mathbf{x})$ and kernel $(K_i)_m$, δ_i is computed with

$$\max \delta_i = \max_{K_i} |\mu((I(\mathbf{x})_m * (K_i)_m)) - \mu(I(\mathbf{x})_m)|. \tag{4}$$

Each δ_i is the absolute distance between an averaged image region $I(\mathbf{x})_m$ and the averaged response of kernel $(K_i)_m$. The enhanced image values I_{enh} are computed with

$$I(\mathbf{x})_{enh} = \begin{cases} I(\mathbf{x}) + \max \delta_i & \text{if } I(\mathbf{x}) \geq \mu(I(\mathbf{x})_m) \\ I(\mathbf{x}) - \max \delta_i & \text{else.} \end{cases} \tag{5}$$

This increases the contrast, because the difference of image values and their neighborhood's average is further increased or decreased. We defined $\sigma = m$ to adjust the Gaussian convolution to the stick kernel's width.

In summary, to enhance lung blood vessels in native, low-dose CT scans, the slices are first smoothed with a Gaussian convolution and then the aforementioned maximum response approach is combined with stick filter kernels. Formally, this yields

$$I(\mathbf{x})_{enh} = I(\mathbf{x}) \pm \max \delta_i(I(\mathbf{x}) * G(\mathbf{x}; \sigma)). \tag{6}$$

We implemented our method in MATLAB and used the *Vesselness* (Sato et al.) and *HessianFilter* (Frangi et al.) modules in MeVisLab 2.8.2 [Ritter, F and Boskamp, T and Homeyer, A et al., 2011].
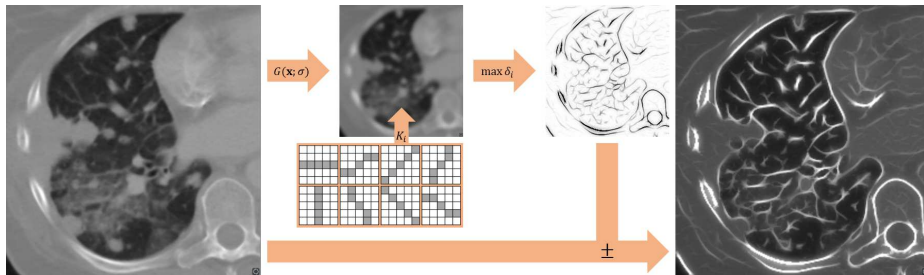

Figure 1: The image processing pipeline of our method. First, the image is blurred with a Gaussian convolution $G(\mathbf{x}, \sigma)$ and then the Stick kernels $(K_i)_m$ are applied with $\sigma = m = 5$. Finally, the enhanced vessels are added to the input image. We inverted the enhanced vessels' visualization for presentation purposes.

Table 1: The processing times of the aforementioned methods for each data set. Each slice has the dimensions of 512×512 pixels. The times were averaged for five executions.

Dataset	Slices	Execution Time (s)		
		Sato et al.	Frangi et al.	Our method
No. 1	117	6.45	3.25	34.49
No. 2	117	6.84	3.24	34.10
No. 3	108	5.83	2.98	31.25
No. 4	107	5.81	2.97	31.89
No. 5	63	3.44	1.75	18.65
Time per Slice (s)		0.05	0.03	0.29

3 Results

Figure 2 shows two image series. This overview depicts the original image, the results of Sato and Frangi et al.'s methods, and the results of our method. The orange-framed image regions are magnified to show the results of all methods in more detail. Additionally, Figure 3 shows two enhanced vessel branchings from the second series in more detail. All our results were obtained with $m = 7$.

All methods were tested on five datasets and the respective processing times are listed in Table 1. We measured them with an i5-2500 processor with 3.70 GHz. Although our method can only be applied on single slices, the methods of Sato and Frangi et al. can be used on image stacks, too. Therefore, all results were acquired using implementations that process single images. We did not use parallel programming methods for any method.

We applied all methods on five datasets. They all have a kilovoltage Peak of 120 kVp and an X-ray tube current between 40 and 80 mA. The acquisition parameters from the low-dose CT scans that were used in the National Lung Screening Trial lie in the same range [National Lung Screening Trial Research Team, 2011].

4 Discussion

We evaluated our method by interviewing two clinical experts. The first interviewee is a Medical Technical Assistant (MTA) with 21 years of working experience in multiple clinical and technical environments. Eight years of that time she worked with CT scans and two years of that time she specifically worked with lung CT scans. When asked, she assessed her anatomical knowledge about the human lung to be fair. Our second interviewee is an assistant doctor with four years of clinical experience. Three and a half years of that time with CT scans and three years of that time specifically with lung CT scans. He reported his anatomical knowledge about the lung to be very good.

They were asked to compare all methods' results and to assess our method's clinical feasibility and possible application areas. We developed a software tool to enable them to explore the original scan and all result images. To support the comparison of multiple image data sets, the zooming, translation, and slicing features and the cursor position were synchronized for multiple views. We did not synchronize the transfer function, because, in general, the value ranges of the original and result images are different.

They stated that the enhancement of large vessels, vessel branches, and lesions is comparable, but our method enhanced mid-size and small vessels more clearly (Fig. 3). Furthermore, they assessed that although small and very thin vessels are visible in the original images, Sato and Frangi et al.'s methods split them while our method connects and enhances them anatomically correct. In summary, they assessed our method to be more suitable to separate blood vessels from surrounding parenchyma. Because of the different processing times (Tab. 1), we prepared our method's results beforehand. We asked them to evaluate the execution times and both stated that they are sufficient.

Both experts stated that our method improves the diagnostic and therapy planning value for low-dose CT scans. Finally, the MTA reported that our method would be beneficial for manual segmentations of lung vessels.

4.1 Limitations and Future Work

We introduced the LANCELOT method that can enhance smaller vessels than Sato and Frangi et al.'s methods, but if σ and m is small, it also enhances image noise (Fig. 2). Our method also enhances the edges of nodules, but they can be distorted (Fig. 3). This could be a problem for nodule detection and segmentation algorithms [Kuhnigk, J-M and Dicken, V and Bornemann, L et al., 2006]. Therefore, they should be applied to the original images rather than our result images to prevent artifacts.

In the future we want to work on three extensions. First, the stick filter kernels should be extended to 3D to include spatial information about blood vessels and second, the processing times can be improved via parallel programming, e. g. on the GPU. Finally, our method computes the $\max \delta_i$ for multiple stick kernels of the same size m and it would be interesting to see which results can be achieved when a multi-scale approach is used, where kernels of different sizes are included, too.

References

[Bresenham, J E, 1965] Bresenham, J E (1965). Algorithm for computer control of a digital plotter. *IBM Systems Journal*, 4(1):25–30.

[Czerwinski, R N and Jones, D L and O'brien, W D, 1998] Czerwinski, R N and Jones, D L and O'brien, W D (1998). Line and Boundary Detection in Speckle Images. *IEEE Trans Image Process*, 7(12):1700–1714.

[Frangi, A F and Niessen, W J and Vincken, K et al., 1998] Frangi, A F and Niessen, W J and Vincken, K et al. (1998). Multiscale vessel enhancement filtering. In *Med Image Comput Comput Assist Interv*, pages 130–137. Springer.

[Kuhnigk, J-M and Dicken, V and Bornemann, L et al., 2006] Kuhnigk, J-M and Dicken, V and Bornemann, L et al. (2006). Morphological Segmentation and Partial Volume Analysis for Volumetry of Solid Pulmonary Lesions in Thoracic CT Scans. *IEEE Trans Med Imaging*, 25(4):417–434.

[Kuhnigk, J-M and Hahn, H and Hindennach, M et al., 2003] Kuhnigk, J-M and Hahn, H and Hindennach, M et al. (2003). Lung lobe segmentation by anatomy-guided 3d watershed transform. In *Proc SPIE*, volume 5032, pages 1482–1490.

[National Lung Screening Trial Research Team, 2011] National Lung Screening Trial Research Team (2011). The National Lung Screening Trial: Overview and Study Design. *Radiology*.

[Ritter, F and Boskamp, T and Homeyer, A et al., 2011] Ritter, F and Boskamp, T and Homeyer, A et al. (2011). Medical Image Analysis. *IEEE Pulse*, 2(6):60–70.

[Rudyanto, R D and Kerkstra, S and Van Rikxoort, E M et al., 2014] Rudyanto, R D and Kerkstra, S and Van Rikxoort, E M et al. (2014). Comparing algorithms for automated vessel segmentation in computed tomography scans of the lung: the VESSEL12 study. *Med Image Anal*, 18(7):1217–1232.

[Sato, Y and Nakajima, S and Atsumi, H et al., 1997] Sato, Y and Nakajima, S and Atsumi, H et al. (1997). 3D Multi-Scale Line Filter for Segmentation and Visualization of Curvilinear Structures in Medical Images. In *CVRMed-MRCAS'97*, pages 213–222. Springer.
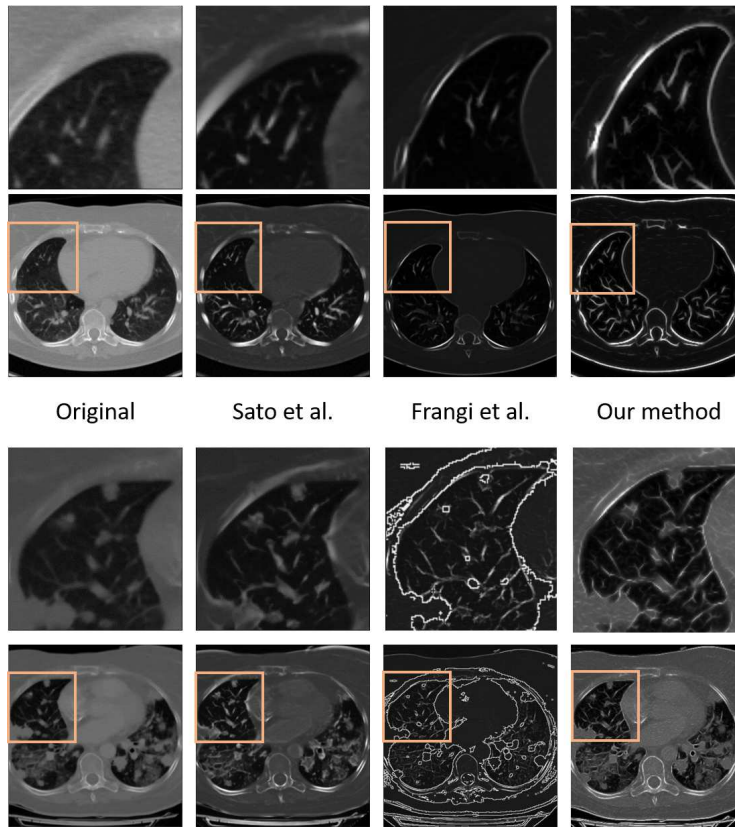
Figure 2: These series show the original images and the results of the aforementioned methods. The framed image regions were magnified for presentation purposes. We used 7×7 filter kernels for our results.
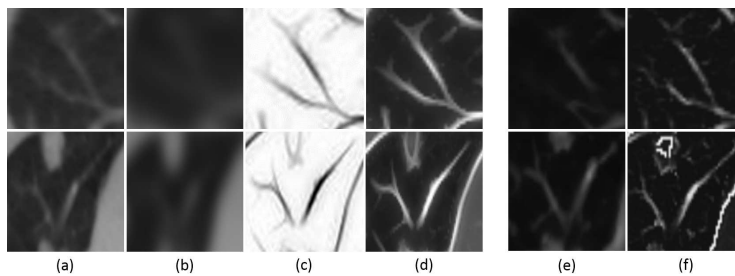

Figure 3: This figure shows the (a) original input image and the interim results after (b) Gaussian convolution, (c) computation of $\max \delta_i$, and (d) when the enhanced vessels were merged with the original image. The last two images show emphasized image regions after the methods from (e) Sato and (f) Frangi et al. were applied.